

Multi-criterion model ensemble of CMIP5 surface air temperature over China

Tiantian Yang¹  · Yumeng Tao¹ · Jingjing Li² · Qian Zhu³ · Lu Su⁴ · Xiaojia He⁵ · Xiaoming Zhang⁶

Received: 12 December 2016 / Accepted: 13 April 2017 / Published online: 15 May 2017
© Springer-Verlag Wien 2017

Abstract The global circulation models (GCMs) are useful tools for simulating climate change, projecting future temperature changes, and therefore, supporting the preparation of national climate adaptation plans. However, different GCMs are not always in agreement with each other over various regions. The reason is that GCMs' configurations, module characteristics, and dynamic forcings vary from one to another. Model ensemble techniques are extensively used to post-process the outputs from GCMs and improve the variability of model outputs. Root-mean-square error (RMSE), correlation coefficient (CC, or R) and uncertainty are commonly used statistics for evaluating the performances of GCMs. However, the simultaneous achievements of all satisfactory statistics cannot be guaranteed in using many model ensemble techniques. In this paper, we propose a multi-model ensemble framework, using a state-of-art evolutionary multi-objective

optimization algorithm (termed MOSPD), to evaluate different characteristics of ensemble candidates and to provide comprehensive trade-off information for different model ensemble solutions. A case study of optimizing the surface air temperature (SAT) ensemble solutions over different geographical regions of China is carried out. The data covers from the period of 1900 to 2100, and the projections of SAT are analyzed with regard to three different statistical indices (i.e., RMSE, CC, and uncertainty). Among the derived ensemble solutions, the trade-off information is further analyzed with a robust Pareto front with respect to different statistics. The comparison results over historical period (1900–2005) show that the optimized solutions are superior over that obtained simple model average, as well as any single GCM output. The improvements of statistics are varying for different climatic regions over China. Future projection (2006–2100) with the proposed ensemble method identifies that the largest (smallest) temperature changes will happen in the South Central China (the Inner Mongolia), the North Eastern China (the South Central China), and the North Western China (the South Central China), under RCP 2.6, RCP 4.5, and RCP 8.5 scenarios, respectively.

✉ Tiantian Yang
tiantiy@uci.edu

¹ Department of Civil and Environmental Engineering, University of California, Irvine, CA 92697, USA

² Department of Geosciences and Environment, California State University, Los Angeles, LA 90032, USA

³ Institute of Hydrology and Water Resources, College of Civil Engineering and Architecture, Zhejiang University, Hangzhou 310058, China

⁴ College of Global Change and Earth System Science, Beijing Normal University, Beijing 100875, China

⁵ The Administrative Center for China's Agenda21, Beijing 100038, China

⁶ State Key Laboratory of Simulation and Regulation of Water Cycle in River Basin, China, Institute of Water Resources and Hydropower Research (IWRH), Beijing 100048, China

1 Introduction

It has been a growing interest in assessing the surface air temperature (SAT) of Global Coupled Atmosphere–Ocean Circulation Models (GCMs) over different regions in the field of climate change and natural resources management. Currently, a number of GCMs with various resolutions and modules are developed and maintained by universities, government agencies, and non-profit organizations around the world. The SAT, as one of the major outputs from GCMs, is able to cause crucial changes in many aspects of society,

including water availability and supply (Piao et al. 2007; Gosling et al. 2011; Miao and Ni 2009; Miao et al. 2014; Sheffield et al. 2012; Sun et al. 2014a; Yang et al. 2016, 2017), food security (Tubiello et al. 2007; Lobell et al. 2008; Piao et al. 2010), ecological environment (Allan et al. 2013; Allen et al. 2010; Miao et al. 2010; Tabari and Hosseinzadeh Talaei 2013; Wu et al. 2017a, b), human health (Robine et al. 2008; Gosling et al. 2009), biological diversity (Wake and Vredenburg 2008; de Oliveira et al. 2014), and so on. According to the recent Fifth Assessment Report (AR5) of the Intergovernmental Panel on Climate Change (IPCC) (IPCC 2007, 2013), the projected SAT will more or less increase in the next century all over the world, especially under the highest greenhouse gas emission scenario or the Representative Concentration Pathway 8.5 (RCP8.5) scenario. The projected SAT increase has urged decision makers to adjust their current natural resources management and development plans and prepare in advance of the temperature-induced consequences of potential drought, increasing water demands, and hydroclimate events. However, it has been noticed that the performances of GCMs are not always in agreement with each other during both historical simulations and future projections (Sun et al. 2014b; Coquard et al. 2004; Phillips and Gleckler 2006; Räisänen 2007; Giorgi and Coppola 2010; Sun et al. 2015). The performance disagreement of among GCMs is well acknowledged, and it impedes a broader and practical use of GCMs among public communities, decision makers, and scientists. To comprehensively evaluate the performances of GCMs, it is recommended by many researchers (Miao et al. 2014; Duan and Phillips 2010; Giorgi and Francisco 2000a, b; Gleckler et al. 2008) that the a comprehensive evaluation on the GCMs' outputs should include multiple statistical measures at the same time, such as root-mean-square error (RMSE), CC (R), and uncertainty. This is because single statistic measure has its own pros and cons, which cannot systematically reveal the intrinsic characteristics of model outputs.

In order to better utilize the GCMs' outputs and improve their prediction reliability (Tebaldi and Knutti 2007), a number of multi-model ensemble techniques have been invented. Those model ensemble techniques are designed to post-process the GCMs' outputs and, therefore, to derive a weighted solution, which is as close as to observation with respect to a user-defined criterion. Some popular methods are the simple model average (SMA) (Hagedorn et al. 2005), Bayesian model average (BMA) (Duan and Phillips 2010; Min and Hense 2006, 2007; Miao et al. 2013), reliability ensemble average (REA) (Giorgi and Mearns 2002; Torres and Marengo 2013), etc. In general, the multi-model ensemble approach is able to generate an ensemble solution that is superior than any single model's output by equally or unequally assigning weights to each participating model (Reichler and Kim 2008; Robertson et al. 2004; Weigel et al. 2008; Lambert and Boer 2001;

Fischer et al. 2012; Buser et al. 2009). The most significant advantages of using multi-model ensemble techniques lie in its capability of reducing model uncertainty, i.e., the deviation range between simulation and observation (Miao et al. 2014; Giorgi and Francisco 2000a; Zanis et al. 2009), and in improving model outputs' reliability (Feng et al. 2011). Typically, only one best ensemble output will be produced using those above referred multi-model ensemble techniques. The ultimate single ensemble solution is not able to reveal multiple aspects of model performances and provide any trade-off information between another ensemble solution. According to the personal communication with many scientist and engineers at the China Meteorology Administration, operating agencies use GCMs' outputs in a prudential manner, in which the different ensemble solutions with various weighting schemes are always compared, tested, and validated against observation before application. The weights to the final ensemble solution are selected by an instrumental mean among various different combinations of weights. Therefore, an automatic ensemble technique is required to have the capability of deriving multiple equivalently important ensemble solutions, as well as the capability of revealing the trade-off information among multiple evaluation criteria with respect to a single ensemble solution. Traditionally, to evaluate the multiple aspects of the performances of GCMs, the Taylor diagram (Taylor 2001) is commonly used. The Taylor diagram is a 2-D plot that concisely summarizes how well a pattern matches the observation in terms of their correlation, root-mean-square difference, and the ratio of their variances (Taylor 2001). A Taylor diagram is constructed based on the geometric relationship (cosine law) between the CC (R), the centered root-mean-square error (RMSE), and the standard deviations of between the simulation and observation. In a two-dimensional Taylor diagram, multiple statistical measures can be shown and evaluated. However, there are only two independent indices included in the Taylor diagram. The axis in a Taylor diagram indicates that once any two statistical indices are set, the third one will be determined by the geometric relationship (cosine law). In other words, there are only two independent measures in a Taylor diagram. If more independent statistical measures, such as uncertainties, are being required in the model evaluation, a new framework is needed to jointly present a third independent statistics in the same plot.

With regard to these concerns, in this paper, we apply a state-of-art multi-objective optimization algorithm, termed multi-objective shuffled complex evolutionary global optimization with principle component analysis and crowding distance (MOSPD) (Yang et al. 2015), to derive multiple GCM ensembles and demonstrate the trade-offs among various solutions. According to Yang et al. (2015), the newly developed MOSPD algorithm combines (1) the strengths of the MOCOM algorithm (Yapo et al. 1998), (2) the concept of the crowding distance-based offspring selection probability

strategy (Deb 2001), and (3) the tool of principal component analysis (Hotelling 1933, 1936) that restores and maintains the population diversity during searching. The MOSPD algorithm is effective and efficient in solving reservoir operation problems, and it is competitive as it compares with other evolutionary searching algorithms over many test functions. The advantages of using MOSPD are that (1) the evolutionary-based searching characteristics allow multiple solutions being derived simultaneously in a single run and (2) it is capable of dealing high-dimensional problems and extensively exploiting the objective space so that most of the extreme solutions can be obtained. From the application point of view, these advantages of MOSPD fit the goal of incorporating more independent statistics in the GCM ensemble evaluation because (1) the weight space is high dimensional and (2) the optimization run can generate a set of ensemble solutions simultaneously in a single run. Therefore, in this paper, we test out the robustness and capability of the newly developed MOSPD algorithm in ensemble various GCMs' outputs.

In the multi-objective optimization context, there will be a set of optimized solutions instead of one single solution that outperforms the rests. Within this set of solutions, one solution cannot be defined as a better solution than another one, as they are equally "good" with respect to each other. Those equally good or important solutions are called non-dominated solutions (Deb 2001). According to Deb (2001), a solution x_1 is said to be dominating to another solution x_2 if the following two statements are true: (1) The solution x_1 is no worse than x_2 in all objectives and (2) the solution x_1 is strictly better than x_2 in at least one objective. It means that to move from one solution to any other solutions, at least one objective function value has to be sacrificed/worsen in order to obtain a better value in other objective functions. Therefore, the optimized non-dominated solutions reveal the trade-off information with respect to multiple competing objectives. In a GCM ensemble example, if considering different statistical measures (i.e., RMSE, CC, and uncertainty) as objective functions, at least one statistical measure will be compromised in order to reach a better performance in another aspect. In other words, the improvement of RMSE will result in the deterioration of at least one other statistics if moving from one ensemble solution with low RMSE towards another one with high RMSE. Furthermore, by displaying the non-dominated solutions in a single plot, a robust line (for two objective functions) or surface (for more than two objective functions) will be formed. This line or surface is commonly called the "Pareto front." The global Pareto front directly demonstrates the conflicting relationship among multiple objective functions. Using the Pareto front to convey the trade-off information is intuitive and straightforward. The adding of additional independent statistical measure in the model evaluation could further help policy makers in selecting an acceptable solution for making an effective climate change adaptation plan.

The advantage of using multi-objective optimization in the GCM ensemble problem lies in two aspects. First, by picturing the Pareto front of optimized ensemble solutions, decision makers/users are able to gain a comprehensive understanding about both the pros and cons of any single ensemble solution. Differing from the Taylor diagram, more independent measurements are able to be included in this framework. For example, a 3-D Pareto front, including RMSE, CC, and model uncertainty as evaluation criteria, is more comprehensive than a 2-D evaluation approach, which is similar to a Taylor diagram. In addition, the Pareto front is also able to provide the quantifications of the differences between a selected solution and its alternatives. With the purpose of extending to a broader use of GCMs by water agencies, the application of the multi-objective optimization algorithm on model ensemble is able to assist policy makers in selecting a more comprehensive decision in mitigating the conflicts among multiple stakeholders or interested parties.

In this paper, a case study over seven geographical regions of China is conducted, in which we use the SAT outputs from 24 GCMs to develop the ensemble. The proposed MOSPD algorithm is applied on the weight tuning process to produce the final non-dominated solutions. The ensemble results derived with MOSPD are compared with the observations, as well as the results from SMA. We further carry out a statistical analysis on the weight distribution obtained from the optimized solutions. The simulation results in historical period (1900–2005) show that the non-dominated solutions derived from MOSPD are superior to both SMA and any single model result with lower RMSE values, higher CC values, and smaller uncertainty range. However, there are still certain systematic biases between ensemble results and observations. During the prediction period (2006–2100), we find that the largest increases are 1.01 °C/100 years in region 2, 2.40 °C/100 years in region 7, and 5.67 °C/100 years in region 5 under RCP 2.6, RCP 4.5, and RCP 8.5 scenarios, respectively. The smallest increases happen in region 6 (0.74 °C/100 years), region 3 (1.75 °C/100 years), and region 2 (4.19 °C/100 years), under RCP 2.6, RCP 4.5, and RCP 8.5 scenarios, respectively.

The contributions of this paper are (1) introducing an application of a newly developed multi-objective optimization framework to derive multi-model ensemble solutions which are better than SMA and contain more comprehensive information of ensemble solutions; (2) extending the application of the newly developed MOSPD algorithm to the field of climate change and multi-model ensemble; and (3) evaluating the model ensemble performances over China in a comprehensive perspective, therefore, to provide policy maker auxiliary information about ensemble solutions.

This paper is organized into six sections: Section 2 describes the study region and data. The optimization model for the GCM ensemble problem and the multi-objective optimization algorithm is introduced in Section 3. In Section 4, the

historical SAT simulation and projection results are shown. Section 5 presents the discussions and conclusions. Finally, the limitations and future works are addressed in Section 6.

2 Study region and data

In this paper, the study region is China located between 15°–55° N and 70°–135° E. It has been reported that the climate in China varies considerably in both space and time due to its complex land topography (Gao et al. 2008). There are few studies focusing on predicting the temperature changes in different geographical regions over China. Therefore, we divide the study region (China) into seven sub-regions based on the official geographical classification reported by China Meteorology Administration as shown in Fig. 1. The CMIP5 model ensemble and optimization are individually conducted for each sub-region in order to distinguish the various characteristics of the temperature changes corresponding to different topographies and hydrology.

There are two main datasets used in this study. The first one is the SAT outputs from 24 GCMs (Table 1) from the recent Fifth Assessment Report (AR5) of the Intergovernmental Panel on Climate Change (IPCC). The SAT outputs are the main forcing data, as well as the inputs to the model ensemble optimization model. The second dataset contains the gridded SAT historical records over China, which is considered as the observation and reference in this study. The historical SAT records are obtained from the Climate Research Unit (CRU) Time Series Data archive. The historical data covers the period from 1900 to 2005. Temporal resolution is monthly, and the spatial resolution is $0.5^\circ \times 0.5^\circ$. Figure 2 demonstrates the

averaged mean SAT over the period of 1900 to 2005 using the CRU Time Series Data.

Three RCPs, namely RCP 2.6, RCP 4.5, and RCP 8.5, are used in evaluating the ensemble solution during future projection period (2006–2100). The RCP 2.6, RCP 4.5, and RCP 8.5 are subject to different assumptions that future radiative forcings are 2.6, 4.5, and 8.5 W/m^2 by 2100, respectively. In addition, each RCP scenario indicates different greenhouse gas concentrations. The amounts of greenhouse gas concentration are assumed to be 421, 538, and 936 ppm in the year 2100, for RCP 2.6, RCP 4.5, and RCP 8.5 scenarios, respectively. Each GCM's output is re-gridded to a spatial resolution of $0.5^\circ \times 0.5^\circ$ to match the resolution of CRU observation.

3 Optimization model and algorithm

3.1 Optimization model

The multi-model ensemble optimization problem during the historical period can be mathematically expressed as the following equation:

$$\text{Sim}(t_1, t_2, \dots, t_n) = \sum_{i=1}^m W_i(w_1, w_2, \dots, w_n) \cdot T_i(t'_1, t'_2, \dots, t'_n) \quad (1)$$

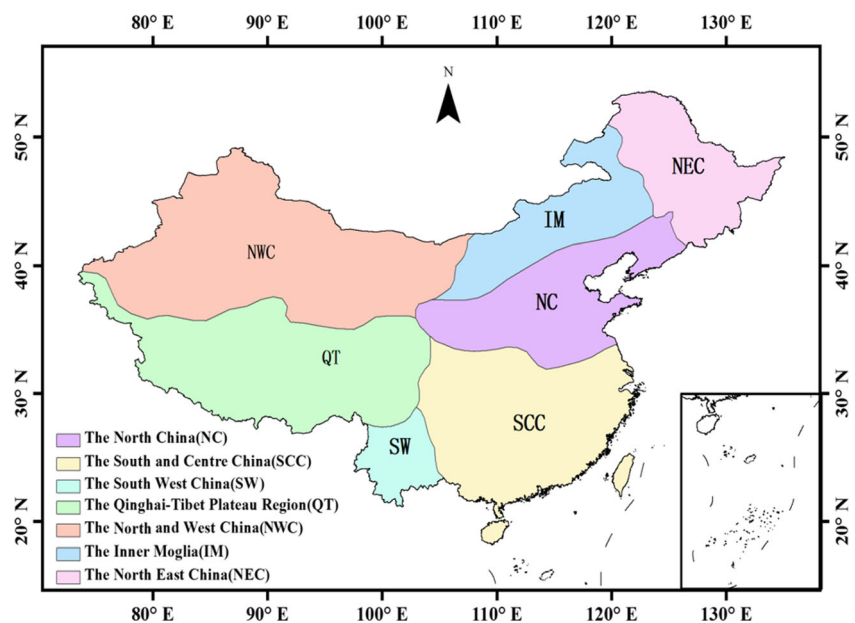
Subject to

$$w_1 + w_2, \dots, +w_m = 1 \quad (2)$$

$$w_j \in [0, 1], j = 1, 2, \dots, m \quad (3)$$

where the vector $\text{Sim}(t_1, t_2, \dots, t_n)$ is the SAT model ensemble, in which t_n is the n th year's mean temperature. The vector $T_i(t'_1, t'_2, \dots, t'_n)$ is the SAT from the output of the i th GCM. m

Fig. 1 The study area classified with different climates over China



is the number of GCMs involved in the ensemble. In this paper, we chose 24 different GCMs; therefore, $m = 24$. w_i represents the weights assigned to each GCM, which is subjected to Eqs. (2) and (3) as constraints. The higher the w_i , the higher the contribution of the i th GCM in constructing the model ensemble $\text{Sim}(t_1, t_2, \dots, t_n)$.

The objective function of the optimization model is set to be optimizing three statistical measurements, namely, RMSE, correlation coefficient (CC), and uncertainty, which describe the differences between the multi-model ensemble vector with the observation vector $\text{Obs}(\tilde{t}_1, \tilde{t}_2, \dots, \tilde{t}_n)$ from various perspectives. As it is shown in the following Eq. (4), the objective functions are (1) to minimize the RMSE, (2) to maximize the CC, and (3) to minimize the uncertainty range. The uncertainty range describes the averaged deviation range between ensemble solution and observation considering the weighted sum of the deviation range for all time steps.

$$\left\{ \begin{array}{l} \min \left(\sqrt{\frac{\sum_{i=1}^n (\tilde{t}_i - t_i)^2}{n}} \right) \\ \max \left(\frac{\sum_{i=1}^n (\tilde{t}_i - \bar{t})(t_i - \bar{t})}{\sqrt{\sum_{i=1}^n (\tilde{t}_i - \bar{t})^2} \sqrt{\sum_{i=1}^n (t_i - \bar{t})^2}} \right) \\ \min \left(\text{average} \left(\left[\frac{\sum_{i=1}^n w_i (T_i - \text{Sim})}{\sum_{i=1}^n w_i} \right]^{1/2} \right) \right) \end{array} \right. \quad (4)$$

where the \bar{t} and \bar{t} represent the mean value of the observation and simulation vector, respectively. Generally, the lower the RMSE value, the less differences in the magnitude between the simulation and observation. The higher the CC, the more similar the variation patterns of the simulation and observation. Similarly, the lower the uncertainty, the less variation of the model ensemble and more confident of the future projections. With regard to the optimization problem defined earlier, the tunable parameters are 24 weights for all the participating GCMs. The parameters are bounded in [0,1] and subjected to the constraints that the sum of the weights equals to 1 (Eqs. 2 and 3).

3.2 Searching algorithm

The searching algorithm used in this paper is a newly developed multi-objective evolutionary optimization algorithm, termed Multi-Objective Shuffled Complex Evolutionary Global Optimization with Principle Component Analysis and Crowding Distance—University of California Irvine (MOSPD-UCI) (Yang et al. 2015). The MOSPD-UCI algorithm

is an updated version of the Multi-Objective Shuffled Complex Evolutionary Global Optimization—University of Arizona (MOCOM-UA) algorithm (Yapo et al. 1998) and also an extension of the single-objective Shuffled Complex Evolution (SCE-UA) global optimization algorithm (Duan et al. 1992). In the MOSPD algorithm, two enhancement modules have been added to the original MOCOM-UA algorithm (Yang et al. 2015). The first module revises the selection possibilities of the members with identical Pareto ranking so that the generated non-dominated solutions can form a more uniformed distribution along the Pareto front. The second module monitors the diversity of the population during evolution based on principal component analysis, which has been shown to prevent the population from degenerating.

The MOSPD-UCI algorithm uses a population-based searching strategy, which generates a set of solution candidates and iteratively updates the candidates until all the candidates are non-dominated to each other. This concept used in MOSPD-UCI is identical to that in MOCOM-UA. According to Yang et al. (2015) and Yapo et al. (1998), the general steps of the evolution can be summarized including the following: (1) a total of $m \times p$ points are randomly sampled in the parameter space to form the initial population, where m is the number of groups (complexes) and p is the total number of individuals in a group (complex); (2) the objective functions are evaluated for each individual; and (3) the entire population is shuffled and split into m groups (complexes). In each of the groups (complexes), the p individuals form the sub-population; (4) the Pareto ranks (Goldberg and Holland 1988) are calculated for the entire population; (5) a triangular possibility function is used to assign a selection possibility to each individual according to its Pareto ranks; (6) the selection possibility for each individual is adjusted according to its crowding distance among the population; (7) a simplex is constructed by selecting $n + 1$ individuals according to the possibility distribution of the sub-population derived from the previous step; (8) the Nelder-Mead evolution strategy (Nelder and Mead 1965) is implemented to obtain a new individual, and the population is updated; (9) the principle component analysis is carried out to check the parameter span in the orthogonal coordinate system and restore the lost dimensions along the axis in the orthogonal coordinate system; and (10) the steps from (3) to (9) are repeated until the maximum of the Pareto ranks in step (4) becomes 1, which means that the individuals in the population are all non-dominated in relation to each other. Detailed descriptions and procedure flowchart of the MOSPD algorithm can be found by Yang et al. (2015) for interested reader.

The following settings are used in applying the MOSPD-UCI algorithm on the multi-model ensemble optimization model (Eqs. 1–3): the number of complexes is 8, the number

Table 1 List of selected CMIP5 Global Circulation Models (GCMs) in this study

GCM No.	Name of model	Spatial resolution	Distribution institute
1	BCC-CSM 1.1	64 × 128	Beijing Climate Center, China Meteorological Administration, China
2	BCC-CSM 1.1 (m)	160 × 320	Beijing Climate Center, China Meteorological Administration, China
3	BNU-ESM	64 × 128	Beijing Normal University, China
4	CanESM2	64 × 128	Canadian Centre for Climate Modelling and Analysis, Canada
5	CCSM4	192 × 288	National Center for Atmospheric Research (NCAR), USA
6	CNRM-CM5	128 × 256	Centre National de Recherches Meteorologiques, France
7	CSIRO-Mk3.6.0	96 × 192	Australian Commonwealth Scientific and Industrial Research Organization
8	FGOALS-g2	108 × 128	Institute of Atmospheric Physics, Chinese Academy of Sciences, China
9	FIO-ESM	64 × 128	The First Institute of Oceanography, SOA, China
10	GFDL-CM3	90 × 144	Geophysical Fluid Dynamics Laboratory, USA
11	GFDL-ESM2G	90 × 144	Geophysical Fluid Dynamics Laboratory, USA
12	GISS-E2-H	90 × 144	Goddard Institute for Space Studies (NASA), USA
13	GISS-E2-R	90 × 144	Goddard Institute for Space Studies (NASA), USA
14	HadGEM2-ES	145 × 192	Met Office Hadley Centre, UK
15	IPSL-CM5A-LR	96 × 96	Institut Pierre-Simon Laplace, France
16	IPSL-CM5A-MR	143 × 144	Institut Pierre-Simon Laplace, France
17	MIROC5	128 × 256	Atmosphere and Ocean Research Institute, University of Tokyo, Japan
18	MIROC-ESM	64 × 128	Japan Agency for Marine-Earth Science and Technology, Atmosphere and Ocean Research Institute (The University of Tokyo), Japan
19	MIROC-ESM-CHEM	64 × 128	Japan Agency for Marine-Earth Science and Technology, Atmosphere and Ocean Research Institute (The University of Tokyo), Japan
20	MPI-ESM-LR	96 × 192	Max Planck Institute for Meteorology (MPI-M), Germany
21	MPI-ESM-MR	96 × 192	Max Planck Institute for Meteorology (MPI-M), Germany
22	MRI-CGCM3	160 × 320	Meteorological Research Institute, Japan
23	NorESM1-M	96 × 144	Norwegian Climate Centre, Norway
24	NorESM-ME	96 × 144	Norwegian Climate Centre, Norway

Source: Miao et al. (2014)

of individuals in 115, the population size is 920, the maximum iteration is 10,000,000, the tunable parameters have a dimension of $n - 1$, where n is the number of GCMs, and the constraint is described in Eq. (1).

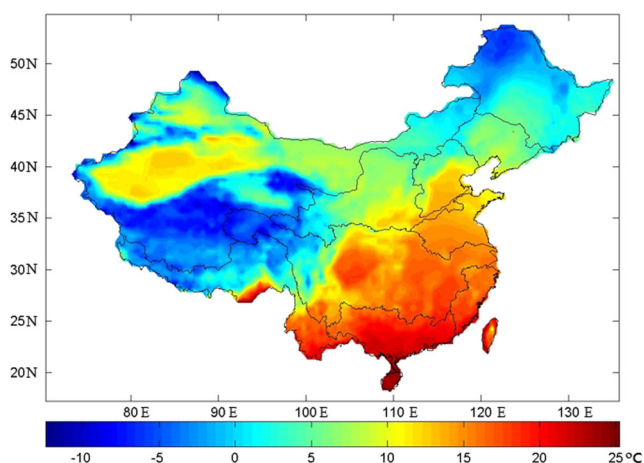


Fig. 2 The averaged mean SAT over the period of 1900 to 2005 using the climate research unit time series data

4 Results and discussion

4.1 Historical simulation

In Fig. 3, the comparison between the optimized non-dominated solutions with MOSPD and the SMA ensemble solution during the historical period (1900–2005) are presented. According to Fig. 3, the non-dominated solutions derived from MOSPD form a robust Pareto front towards the right bottom corner in the objective space (the space created by RMSE, CC, and uncertainty). It is found that the ensemble solutions for different regions are associated with various values of RMSE, CC, and uncertainty as compared to observations. For a better visualization, in Fig. 4, we project the results of region No. 1 (the North Central China) from Fig. 3 into different 2-D objective planes. Figure 4a is exactly the sub-plot for region No. 1 obtained from Fig. 3. Figure 4b–d shows the projected ensemble solutions on the RMSE-uncertainty plane, the correlation-RMSE plane, and the correlation-uncertainty plane, respectively. As it is shown in Fig. 4, there still exist some differences between the optimized

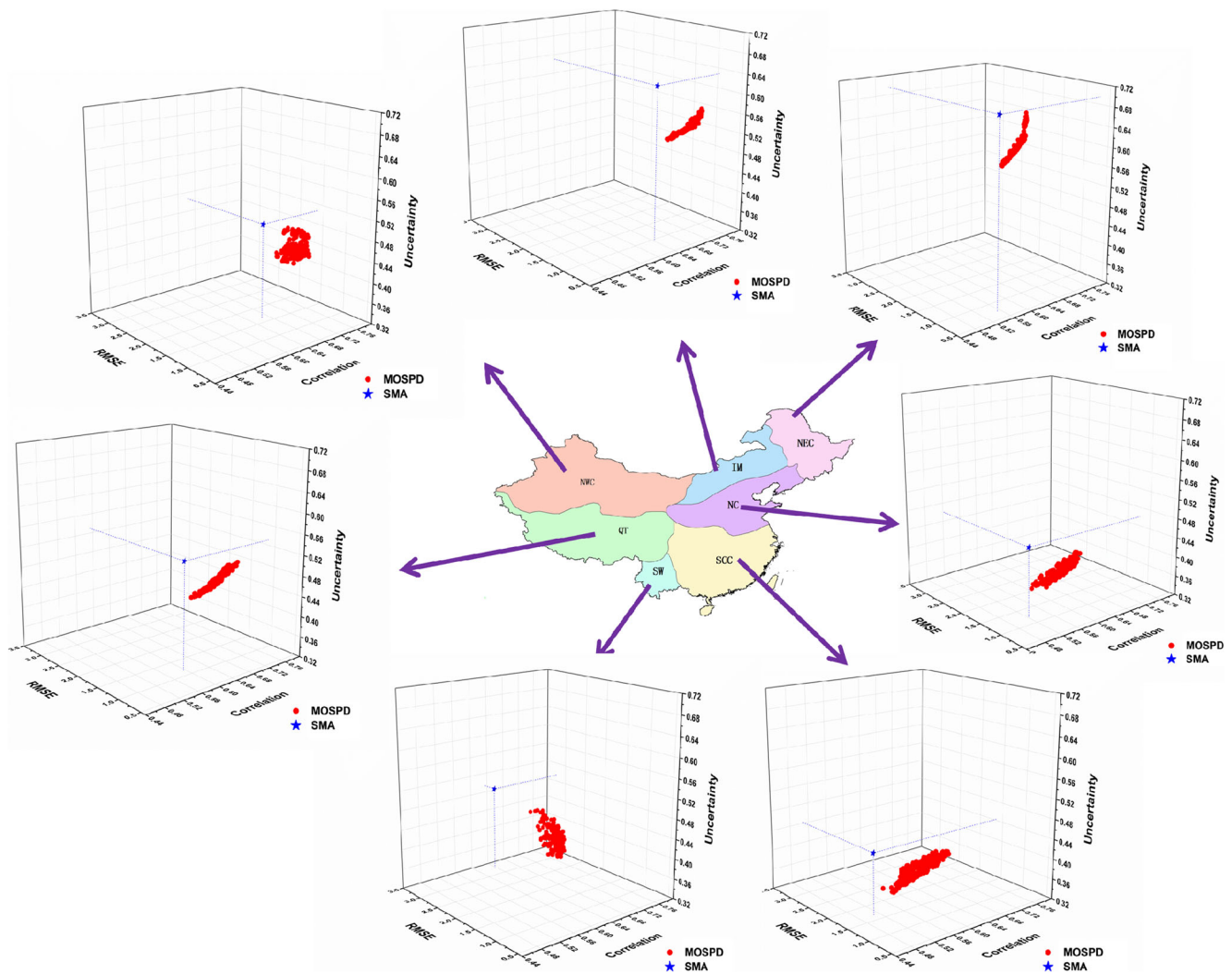


Fig. 3 Historical simulation of the SMA ensemble solution (*blue*) and the non-dominated solutions (*red*) derived from MOSPD over 7 geographical regions in China during 1900–2005

solutions and the theoretical best location, which is located at the corner with RMSE = 0, uncertainty = 0, and correlation coefficient = 1. Nevertheless, the optimized non-dominated solutions have better objective values than that with the SMA ensemble as a baseline.

In order to further verify the model ensemble results derived from MOSPD, both Taylor diagram and skill scores are employed to compare the ensemble solutions with observation. The Taylor diagram provides a direct measurement of the closeness and similarity between the ensemble/individual GCM outputs and the observations. The similarity is measured in terms of their RMSE, CC, and standard deviation (Std). The three statistical indices are presented in a 2-D plot and related by the following cosine law equation:

$$RMS^2 = \sigma_m^2 + \sigma_o^2 - 2\sigma_o\sigma_m R \tag{5}$$

where σ_o and σ_m are the standard deviations of the simulation and observation, respectively (Taylor 2001). The comparison

between the SMA and non-dominated solutions derived from the MOSPD algorithm are shown in Fig. 5. According to Fig. 5, the non-dominated solutions derived with MOSPD are relatively closer to the observation than the result of SMA in 2-D space created by the Taylor diagram. These results are consistent with those shown in previous Figs. 3 and 4, in which the dimension of the objective functions space (i.e., statistical index space) is extended to 3-D.

Furthermore, the skill scores, which measure the differences between the non-dominated solutions derived from the MOSPD algorithm and the SMA, are calculated according to the following Eqs. (6), (7), and (8). The skill scores indicate the percentage of improvement of the solutions derived from the MOSPD algorithm with respect to that obtained from SMA.

$$R \text{ ratio} = 1 - |R_{SMA}/R_{ns}| \tag{6}$$

$$RMSE \text{ ratio} = 1 - RMSE_{ns}/RMSE_{SMA} \tag{7}$$

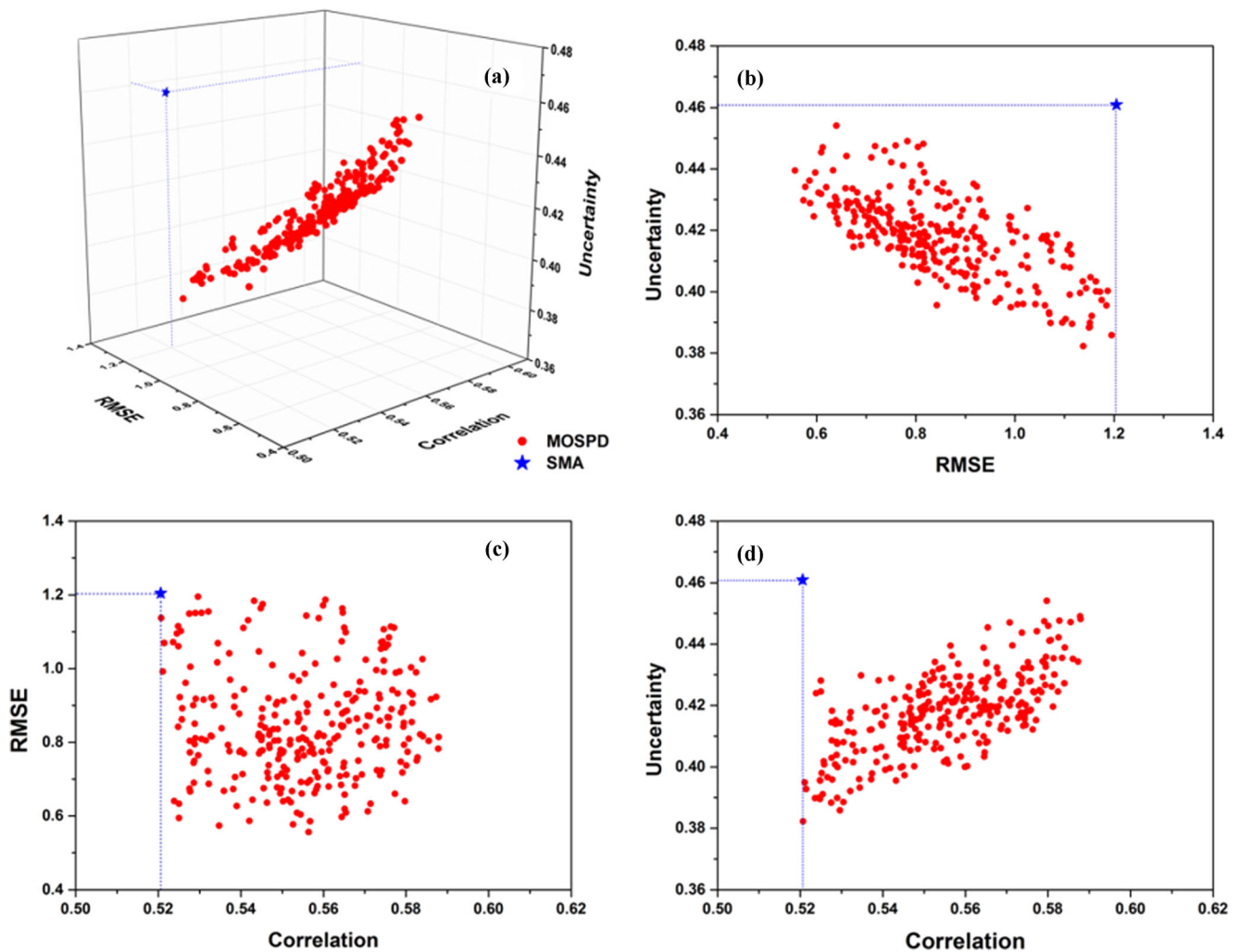


Fig. 4 The SMA ensemble solution (blue) and the non-dominated solutions (red) for region 1 (North Central China) during 1900–2005 in the **a** objective space, **b** RMSE-uncertainty projection plane, **c** correlation-RMSE projection plane, and **d** correlation-uncertainty projection plane

$$\text{Uncertainty ratio} = 1 - \text{Uncertainty}_{ns} / \text{Uncertainty}_{SMA} \quad (8)$$

where ns represents the non-dominated solutions.

As it is shown in previous Figs. 3 and 4, the non-dominated solutions have better RMSE, CC, and uncertainty values than the SMA. Therefore, the R ratio in Eq. (6) is calculated as 1 minus the absolute value of the CC of SMA (R_{SMA}) over the absolute value of the CC of the non-dominated solutions (R_{ns}). Theoretically, if the R_{ns} is greater than R_{SMA} , the R ratio will lie in the range of $(-\infty, 1)$. The closer the R ratio is to 1, the more correlated the non-dominated solutions are to the observation. Similar logic applies to the RMSE and uncertainty ratios (Eqs. 7–8). The RMSE ratio and uncertainty ratio are bounded to $(-\infty, 1]$. The larger the ratio is, the better the performances of non-dominated solutions are over the SMA. The results of the CC, RMSE, and uncertainty ratios are presented in Fig. 6.

Note that in Fig. 4, the derived non-dominated solutions are associated with various combinations of RMSE, CC, and uncertainty. A set of non-dominated solutions will form a robust surface when they are projected on each objective plane (Fig. 5). The philosophy behind this is that no single solution is better than the other because they are equally good with regard to the fitnesses of all objectives, i.e., RMSE, CC, and uncertainty. The ensemble weights for each non-dominated solution are also different, which indicate the contributions of a single model with respect to producing the corresponding ensemble solution. In the following Fig. 7, the distributions of the weights among the derived non-dominated solutions are shown with boxplots. In Fig. 7, the x -axis is the model index as listed in Table 1. The shapes of the boxplots in Fig. 7 indicate the contribution of each participating GCM in producing the non-dominated ensemble solutions. Generally, the higher the center of each weight distribution and the narrower the distribution shape, the better performance and higher

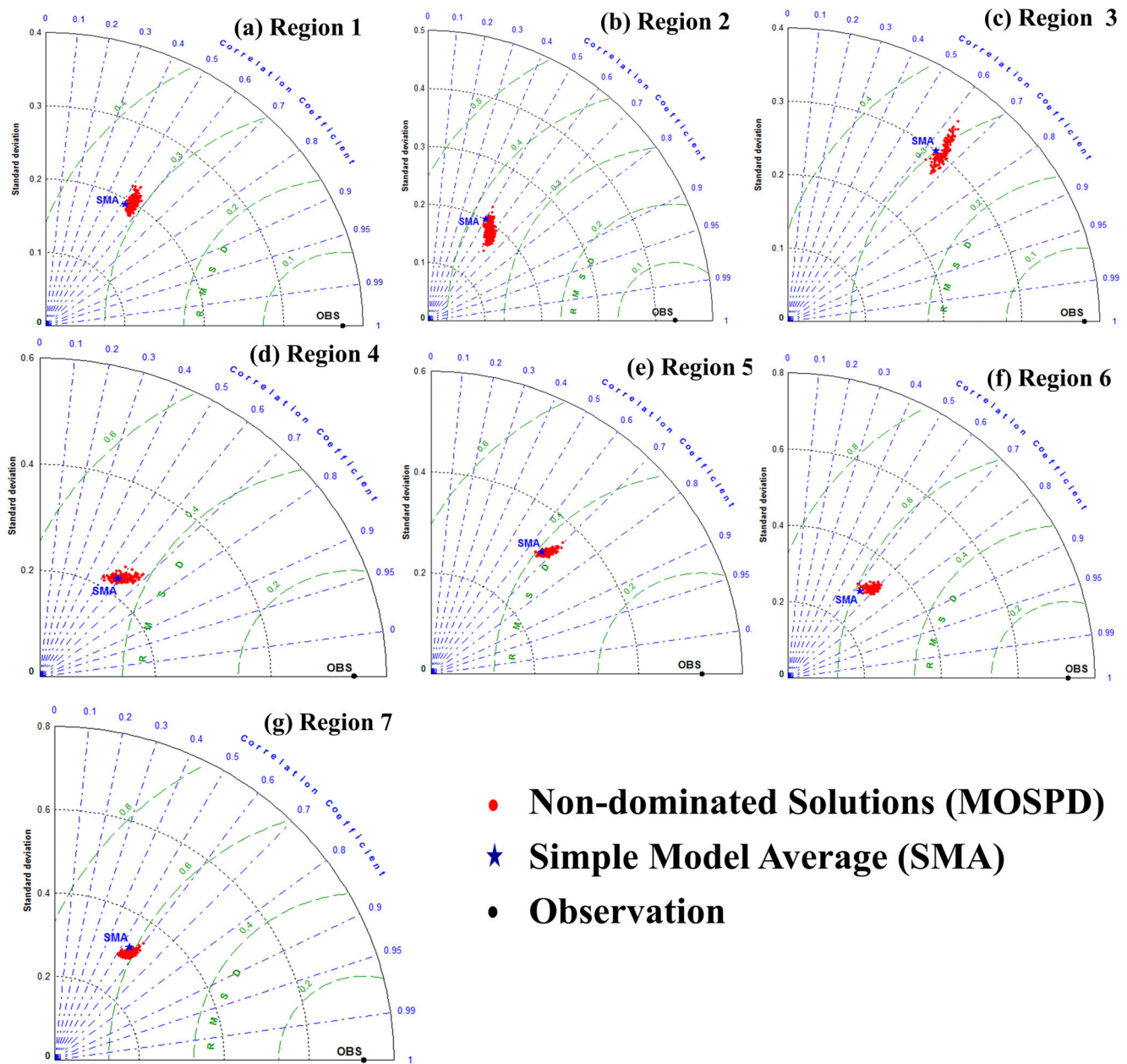


Fig. 5 The Taylor diagram of the results from SMA and the non-dominated solutions with MOSPD for seven geographical regions over China. **a** Region 1. **b** Region 2. **c** Region 3. **d** Region 4. **e** Region 5. **f** Region 6. **g** Region 7

contributions a participating GCM has in producing the optimal ensemble. According to Fig. 7, the mean values and the general shapes of the weight distribution are different from one region to another. It indicates that the performances of individual GCMs are geographically related. One particular GCM, which performs well in a particular region, may not produce consistently reliable and good simulations when applied in another region. Given the fact the output from any single GCM is geographically dependent, it is a tedious task to select a number of different GCMs and perform model ensemble in one region. In addition, a low RMSE value from one ensemble solution does not guarantee the acceptable values

for other statistical measures, such as CC or uncertainty. Using the multi-criterion evaluation approach presented in this paper, and the trade-off information among final non-dominated solutions, decision makers could easily pick the combination of GCMs and the ensemble solution that fits in his/her needs considering the local hydrology in the region of interests. For example, according to the weight distribution shown in Fig. 7, it is able to confidently select models that have higher mean values or better performance for each geographical region. This is because that the higher mean value of the weight of a single model among ensemble candidates indicates that this model has a larger significance and importance in improving

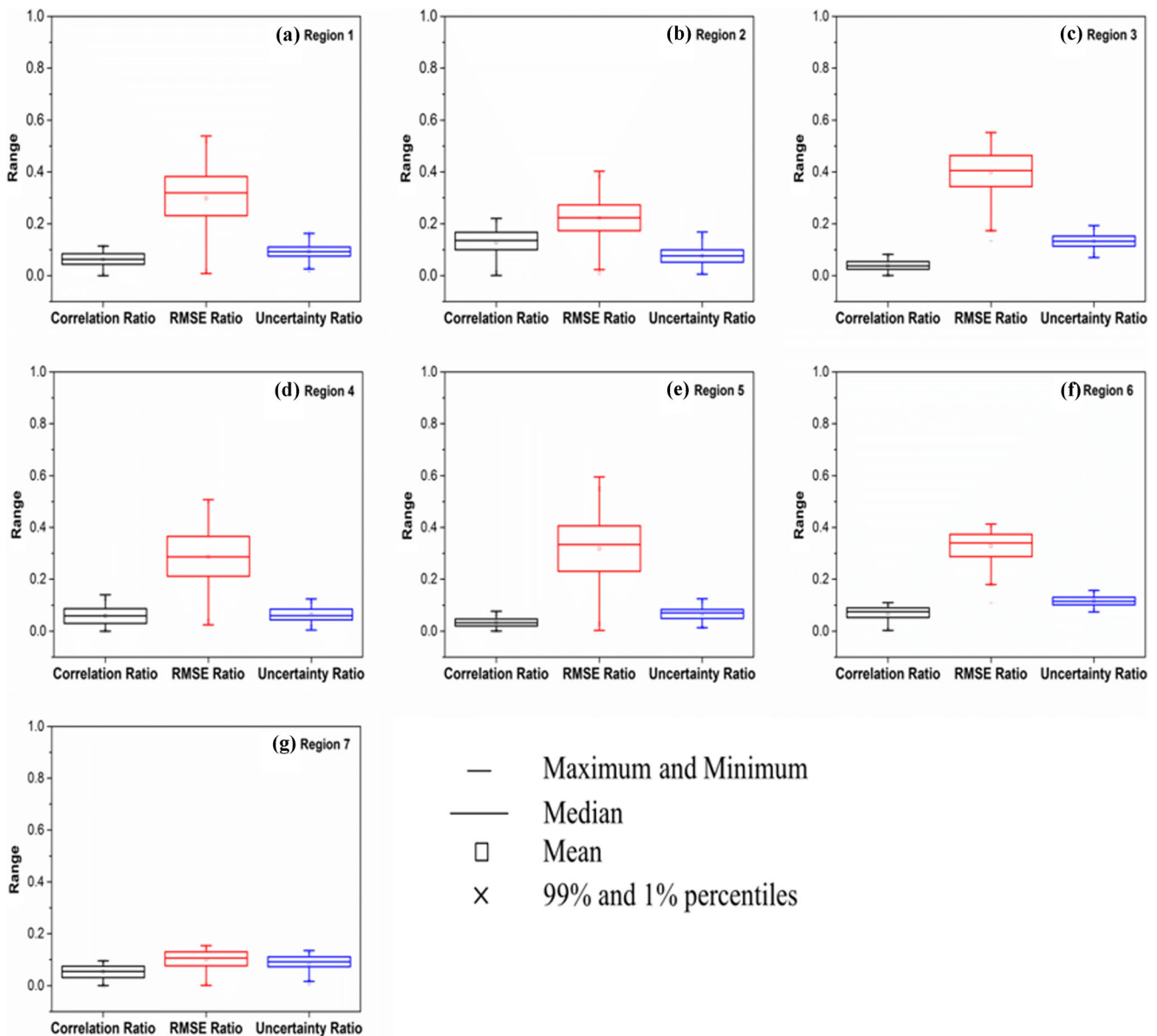


Fig. 6 The correlation, RMSE, and uncertainty ratios of the non-dominated solutions over SMA for seven geographical regions over China. **a** Region 1. **b** Region 2. **c** Region 3. **d** Region 4. **e** Region 5. **f** Region 6. **g** Region 7

statistical performance of ensemble solution than other models. The selection is based on large numbers of non-dominated solutions, which are consistently superior to both individual model and SMA ensemble. Based on the weight distributions shown in Fig. 7, we list the best top 3 models for each geographical region in Table 2. The mean values of the distributions of weights are calculated and used for developing a single ensemble in order to further compare with SMA and observations.

The results of the model ensemble with MOSPD-UCI algorithm (from the mean values), SMA, and observations during the historical period (1900–2005) are shown in Fig. 8. In Fig. 8, both MOSPD-UCI algorithm and SMA tend to underestimate the SAT for all climatic regions over China.

Nevertheless, the results with MOSPD-UCI algorithm are much closer to the observation than the SMA for region Nos. 1–6 (Fig. 8a–f). For region 7 (Fig. 8g), the differences between two methods are negligible. According to our skill score analysis provided in Fig. 6, the MOSPD-UCI algorithm is capable of significantly reducing the RMSE with an approximate percentage of 30% for region Nos. 1–6. But the improvements for region 7 (Fig. 6g) are limited.

In summary, the proposed multi-objective optimization approach has a consistently better performance in deriving

Fig. 7 The weight distribution of the non-dominated solutions for seven geographical regions over China. **a** Region 1. **b** Region 2. **c** Region 3. **d** Region 4. **e** Region 5. **f** Region 6. **g** Region 7

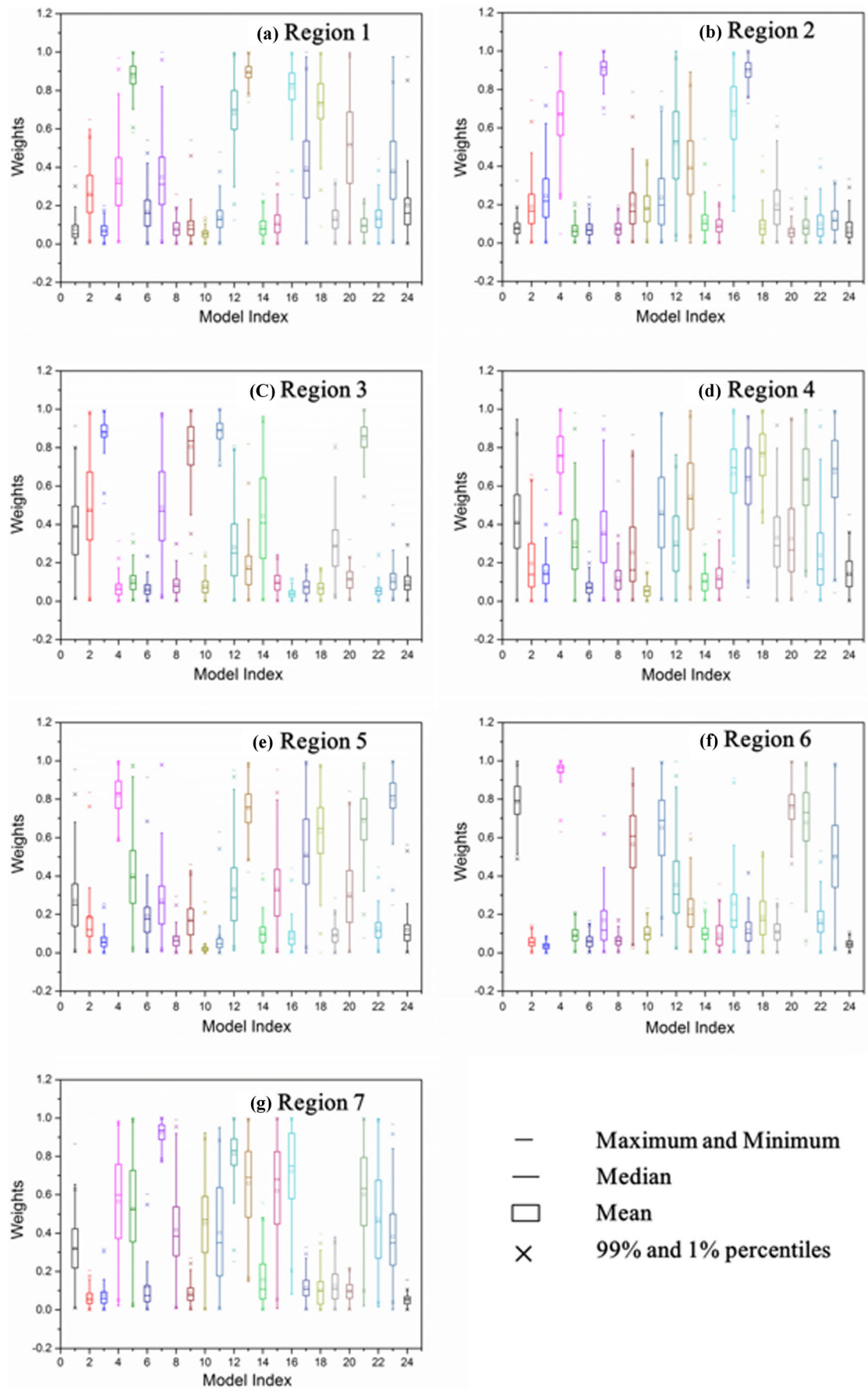


Table 2 The best three models for each geographical region according to the mean values of weight distributions

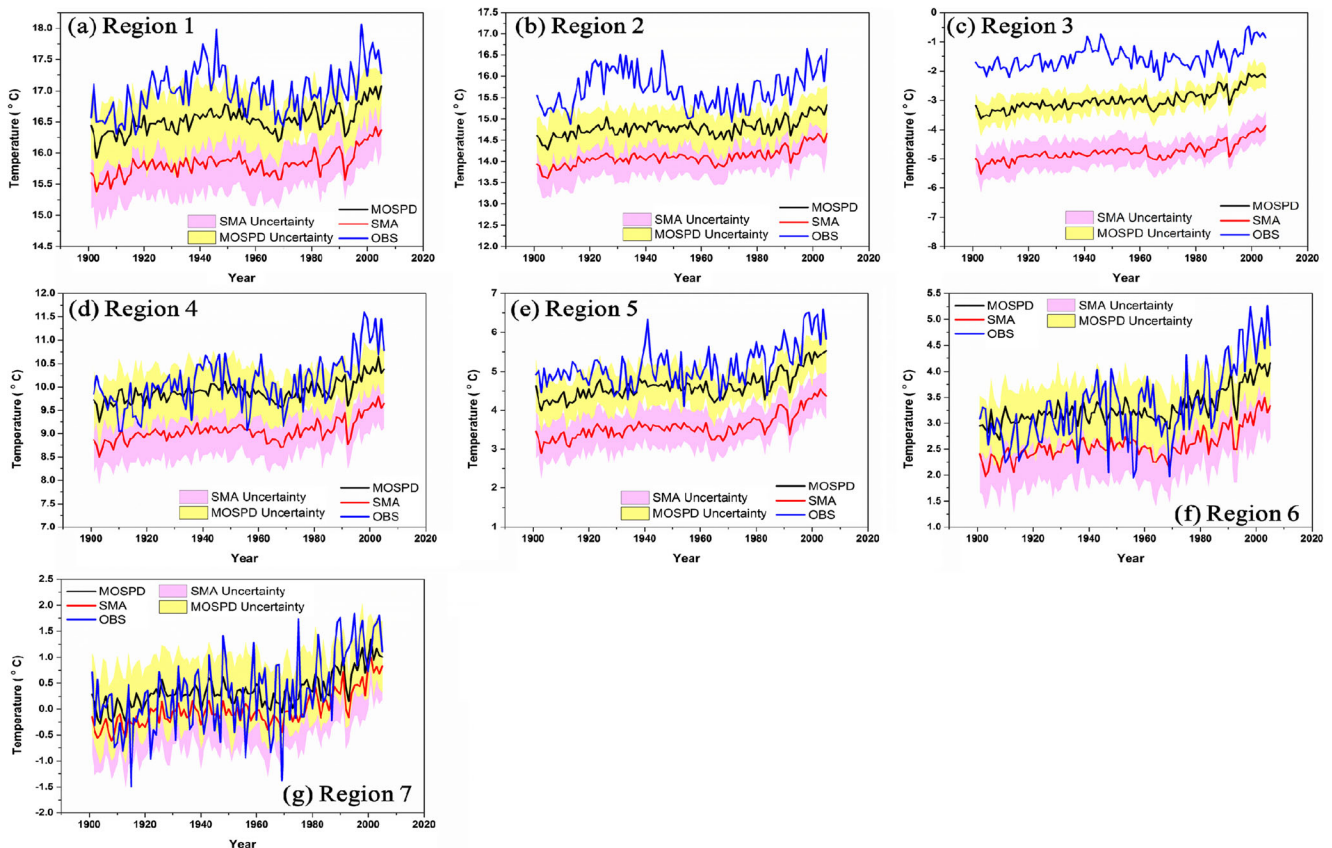
Climate region	Top 1	Top 2	Top 3
1	CCSM4	GISS-E2-R	IPSL-CM5A-MR
2	CSIRO-Mk3.6.0	MIROC5	CanESM2
3	BNU-CSM1.1 (m)	GFDL-ESM2G	MPI-ESM-MR
4	CanESM2	MIROC-ESM	NorESM1-M
5	CanESM2	NorESM1-M	GISS-E2-R
6	CanESM2	BCC-CSM 1.1	MPI-ESM-LR
7	CSIRO-Mk3.6.0	GISS-E2-H	IPSL-CM5A-MR

model ensembles when it is compared to the SMA. The improvements mainly lie in reducing the RMSE between the simulated result and the observation as it is shown in Fig. 6. In addition, the optimal solutions (weight sets) are equally important among all ensemble candidates. According to our study, the argument that one solution is superior to another is questionable, because among the optimized ensemble candidates, the improvement of one objective (either RMSE, CC, or uncertainty) can only be achieved by sacrificing at least one of the other two

objective values. From this point of view, in practical uses of GCM ensemble, it is suggested to have multiple evaluation criterion so that comprehensive understanding about the trade-offs among different ensemble solutions can be utilized in the decision-making process. By evaluating the model contribution among multiple equally important ensemble solutions, a more confident selection of GCMs and a better corresponding climate adaptation plan could be achieved, in which such information will be provided by our proposed multi-objective optimization framework.

4.2 Future projection

Using the same weight combination obtained with the MOSPD algorithm in historical simulation period (1900–2005), we present the model outputs for the projection period (2006–2100) in Fig. 9. The projections are conducted for different regions under low (RCP 2.6), medium (RCP 4.5), and high (RCP 8.5) CO₂ emission scenarios. The average temperature increases over 100 years for each region under each scenario are listed in Fig. 9. According to Fig. 9, the largest increase is 1.01 °C/100 years (region 2), 2.40 °C/100 years (region

**Fig. 8** Comparisons among the model ensemble with MOSPD, SMA, and observation for different regions. **a** Region 1. **b** Region 2. **c** Region 3. **d** Region 4. **e** Region 5. **f** Region 6. **g** Region 7

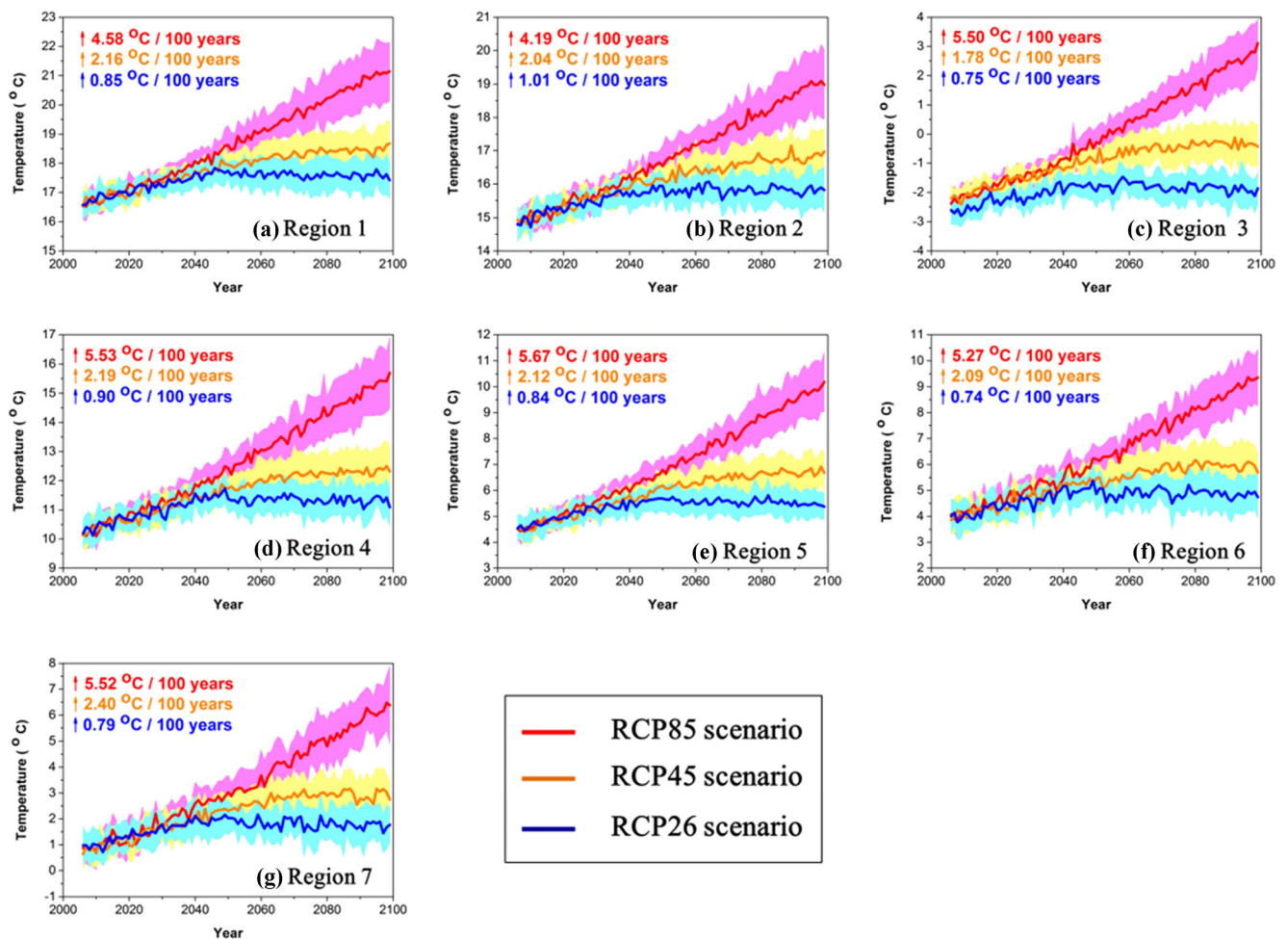


Fig. 9 Future model ensembles for different regions under RCP 2.6, RCP 4.5, and RCP 8.5 CO₂ emission scenarios. **a** Region 1. **b** Region 2. **c** Region 3. **d** Region 4. **e** Region 5. **f** Region 6. **g** Region 7

7), and 5.67 °C/100 years (region 5) under RCP 2.6, RCP 4.5, and RCP 8.5 scenarios, respectively. The smallest increase happens in region 6 (0.74 °C/100 years), region 3 (1.75 °C/100 years), and region 2 (4.19 °C/100 years), under RCP 2.6, RCP 4.5, and RCP 8.5 scenarios, respectively.

Note that the results shown in Fig. 8 are calculated by the mean values of the weight distribution (Fig. 7). Therefore, it cannot be concluded this result will have a best statistical index for each region individually. Nevertheless, the ensemble result derived with the proposed MOSPD-UCI algorithm will be superior to any single model output, as well as the SMA when simultaneously considering all statistical measures (Fig. 6). Furthermore, it can be inferred from Figs. 5 and 8 that the ensemble result using the optimized weights from MOSPD will be closer to the realities in future than the SMA, given the fact that the results from MOSPD consistently perform better than the SMA during the historical period (1900–2005).

5 Conclusion

In this paper, a newly developed multi-objective optimization algorithm, termed MOSPD-UCI algorithm, is applied to derive optimal GCM ensembles with the consideration of many evaluation criterion. A case study over seven geographical regions over China is carried out using the proposed multi-objective ensemble framework. The advantage of using multi-objective optimization algorithm in GCMs multi-model ensemble is that multiple independent aspects of the statistical performances of GCMs, such as the RMSE, CC, and uncertainty, can be simultaneously evaluated. Theoretically, other aspects of GCMs' performances beyond RMSE, CC, and uncertainty, can also be included and tested with the proposed multi-objective optimization scheme. The comparison study during the historical period (1990–2005) shows that the optimized model weights are able to give better model ensemble single model, as well as the SMA method. The ensemble solutions derived with

MOSPD-UCI algorithm have significantly lower RMSE and uncertainty values, and consistently higher CC values, than that with SMA approach in all of our case studies. In details, several conclusions can be drawn as follows:

1. The use of the proposed multi-objective optimization framework to ensemble multiple GCMs' outputs is capable of comprehensively comparing various independent aspects of different behaviors of model. The classical Taylor diagram essentially evaluates only two independent variables among the RMSE, CC, and Std. The third metric is subject to a geometric relationship on the RMSE and CC. This is the reason that visually, only a 2-D plot can be made. In the multi-objective framework, more aspects of GCMs can be compared with the concept of non-dominated solutions and a Pareto front. The 3-D visualization could further help policy makers to better understand the trade-off among different ensembles. From the user's perspective, multiple solutions (weight combinations) enable the user to flexibly select preferred ensemble solution that tailored to their local hydrology.
2. According to the historical simulation (Fig. 8), large biases are associated with GCMs over the entire China. Note that in Fig. 7, the observations do not fall in the envelope of the ensemble uncertainties. This indicates that huge differences still exist between ensemble results and observations. Though the optimized weights with MOSPD tend to produce ensembles with lower RMSE than SMA, the improvements of statistical indices are still limited, especially for the case of region 7. Therefore, it can be concluded that ensemble techniques' major capability is to reduce bias, rather than CC or uncertainty.
3. For the prediction period (2006–2100), the use of MOSPD-UCI algorithm enables an ensemble with more confidence of a less bias, a higher CC value, and a smaller uncertainty range than those produced by the SMA method. This conclusion is made based on the superior performances of MOSPD-UCI algorithm over the SMA method during the historical simulation period (1900–2005). According to Fig. 9, the largest increases and lowest increases under different CO₂ emission scenarios can be found for each region. One interesting finding is that region 2 (South and Central China) is associated with both the largest temperature increases under RCP 2.6 scenario and the smallest increases under the RCP 8.5 scenario. In addition, we calculate the differences of temperature increases between RCP 2.6 and RCP 8.5 scenarios by subtracting the largest temperature increase under RCP 2.6 from that under RCP 8.5 scenarios. Given the fact that future emission scenarios are not certain, our results show that the variations of temperature increases are 3.73, 3.18,

4.75, 4.63, 4.73, 4.53, and 4.73 °C/100 years for regions 1, 2, 3..., and 7, respectively. Note that region 1 (North Central China) and region 2 (South Central China) are the two most populated and developed regions in China. These two regions are associated with the two lowest temperature changes between the "optimistic" (RCP 2.6) and "pessimistic" (RCP 8.5) scenarios. This finding suggests that these two regions have less resilience in response to the increasing CO₂ emissions due to the heavy economic and urbanization development. Human-induced CO₂ emissions in these two regions are already tremendous and relatively higher than other regions. The existing of high-level CO₂ emissions results in less variation of temperature increases under the projection scenarios in IPCC reports.

6 Limitation and future works

The limitations of this study lie in the analysis of finding the extreme solutions among the objective functions. As mentioned in the discussion, the capabilities of GCMs in simulating and projecting temperature over China are limited. The discovery of the extreme weight combination is of great importance in better evaluating the performances of GCMs. Nevertheless, the use of the proposed MOSPD-UCI algorithm is a move towards providing decision makers with a more comprehensive trade-off information for evaluating GCMs' ensemble. Future works are suggested to apply proper techniques with the intention of finding extreme ensemble solutions and to carry out studies on discovering the realistic global Pareto fronts of the model ensembles, as well as adding more evaluation criterion to the multi-objective optimization framework.

Acknowledgements This research was supported by the National Natural Science Foundation of China (No. 41622101), the NASA MIRO grant (NNX15AQ06A) program, and the DOE (Prime Award No. DE-IA0000018). The authors would like to thank anonymous reviewers for their valuable suggestions and comments.

References

- Allan C, Xia J, Pahl-Wostl C (2013) Climate change and water security: challenges for adaptive water management. *Curr Opin Environ Sustain* 5(6):625–632
- Allen CD, Macalady AK, Chenchouni H, Bachelet D, McDowell N, Vennetier M, Kitzberger T, Rigling A, Breshears DD, Hogg E (2010) A global overview of drought and heat-induced tree mortality reveals emerging climate change risks for forests. *For Ecol Manag* 259(4):660–684

- Buser CM, Künsch H, Lüthi D, Wild M, Schär C (2009) Bayesian multi-model projection of climate: bias assumptions and interannual variability. *Clim Dyn* 33(6):849–868
- Coquard J, Duffy P, Taylor K, Iorio J (2004) Present and future surface climate in the western USA as simulated by 15 global climate models. *Clim Dyn* 23(5):455–472
- Deb K (2001) Multi-objective optimization using evolutionary algorithms. Wiley, Hoboken
- de Oliveira JAP, Doll CN, Moreno-Peñaranda R, Balaban O (2014) Global environmental change. Springer, Berlin, pp 461–468
- Duan Q, Phillips TJ (2010) Bayesian estimation of local signal and noise in multimodel simulations of climate change. *J Geophys Res* 115: D18123. doi:10.1029/2009JD013654
- Duan Q, Sorooshian S, Gupta V (1992) Effective and efficient global optimization for conceptual rainfall-runoff models. *Water Resour Res* 28(4):1015–1031
- Feng J, Lee D-K, Fu C, Tang J, Sato Y, Kato H, Mcgregor JL, Mabuchi K (2011) Comparison of four ensemble methods combining regional climate simulations over Asia. *Meteorol Atmos Phys* 111(1–2):41–53
- Fischer A, Weigel A, Buser C, Knutti R, Künsch H, Liniger M, Schär C, Appenzeller C (2012) Climate change projections for Switzerland based on a Bayesian multi-model approach. *Int J Climatol* 32(15): 2348–2371
- Gao X, Shi Y, Song R, Giorgi F, Wang Y, Zhang D (2008) Reduction of future monsoon precipitation over China: comparison between a high resolution RCM simulation and the driving GCM. *Meteorol Atmos Phys* 100(1–4):73–86
- Giorgi F, Coppola E (2010) Does the model regional bias affect the projected regional climate change? An analysis of global model projections. *Clim Chang* 100(3–4):787–795
- Giorgi F, Francisco R (2000a) Evaluating uncertainties in the prediction of regional climate change. *Geophys Res Lett* 27(9):1295–1298
- Giorgi F, Francisco R (2000b) Uncertainties in regional climate change prediction: a regional analysis of ensemble simulations with the HADCM2 coupled AOGCM. *Clim Dyn* 16(2–3):169–182
- Giorgi F, Mearns LO (2002) Calculation of average, uncertainty range, and reliability of regional climate changes from AOGCM simulations via the “reliability ensemble averaging” (REA) method. *J Clim* 15(10):1141–1158
- Gleckler PJ, Taylor KE, Doutriaux C (2008) Performance metrics for climate models. *J Geophys Res* 113:D06104. doi:10.1029/2007JD008972
- Goldberg DE, Holland JH (1988) Genetic algorithms and machine learning. *Mach Learn* 3(2):95–99
- Gosling S, Lowe J, McGregor G, Pelling M, Malamud B (2009) Associations between elevated atmospheric temperature and human mortality: a critical review of the literature. *Clim Chang* 92(3–4): 299–341
- Gosling SN, Warren R, Amell NW, Good P, Caesar J, Bernie D, Lowe JA, van der Linden P, O’Hanley JR, Smith SM (2011) A review of recent developments in climate change science. Part II: the global-scale impacts of climate change. *Prog Phys Geogr* 35(4):443–464
- Hagedorn R, DOBLAS-REYES FJ, Palmer T (2005) The rationale behind the success of multi-model ensembles in seasonal forecasting—I. Basic concept. *Tellus Series a-Dynamic Meteorology and Oceanography* 57(3):219–233
- Hotelling H (1933) Analysis of a complex of statistical variables into principal components. *J Educ Psychol* 24:417–441
- Hotelling H (1936) Relations between two sets of variables. *Biometrika* 28(3–4):321–377
- IPCC (2007) Climate change 2007: the physical science basis. Contribution of Working Group I to the Fifth Assessment Report of the Intergovernmental Panel on Climate Change. Cambridge University Press, Cambridge
- IPCC (2013) Climate change 2013: the physical science basis. Contribution of Working Group I to the Fifth Assessment Report of the Intergovernmental Panel on Climate Change. Cambridge University Press, Cambridge
- Lambert SJ, Boer GJ (2001) CMIP1 evaluation and intercomparison of coupled climate models. *Clim Dyn* 17(2–3):83–106
- Lobell DB, Burke MB, Tebaldi C, Mastrandrea MD, Falcon WP, Naylor RL (2008) Prioritizing climate change adaptation needs for food security in 2030. *Science* 319(5863):607–610
- Miao C-Y, Ni J-R (2009) Variation of natural streamflow since 1470 in the Middle Yellow River, China. *Int J Environ Res Public Health* 6(11):2849–2864
- Miao C, Ni J, Borthwick AG (2010) Recent changes of water discharge and sediment load in the Yellow River basin, China. *Prog Phys Geogr* 34(4):541–561
- Miao C, Duan Q, Sun Q, Li J (2013) Evaluation and application of Bayesian multi-model estimation in temperature simulations. *Prog Phys Geogr* 37(6):727–744
- Miao C, Duan Q, Sun Q, Huang Y, Kong D, Yang T, Ye A, Di Z, Gong W (2014) Assessment of CMIP5 climate models and projected temperature changes over Northern Eurasia. *Environ Res Lett* 9(5):055007
- Min S-K, Hense A (2006) A Bayesian assessment of climate change using multimodel ensembles. Part I: global mean surface temperature. *J Clim* 19(13):3237–3256
- Min S-K, Hense A (2007) A Bayesian assessment of climate change using multimodel ensembles. Part II: regional and seasonal mean surface temperatures. *J Clim* 20(12):2769–2790
- Nelder JA, Mead R (1965) A simplex method for function minimization. *Comput J* 7(4):308–313
- Phillips, T.J. and Gleckler, P.J. (2006) Evaluation of continental precipitation in 20th century climate simulations: the utility of multimodel statistics. *Water Resour Res* 42(3).
- Piao S, Friedlingstein P, Ciais P, de Noblet-Ducoudré N, Labat D, Zaehele S (2007) Changes in climate and land use have a larger direct impact than rising CO₂ on global river runoff trends. *Proc Natl Acad Sci* 104(39):15242–15247
- Piao S, Ciais P, Huang Y, Shen Z, Peng S, Li J, Zhou L, Liu H, Ma Y, Ding Y (2010) The impacts of climate change on water resources and agriculture in China. *Nature* 467(7311):43–51
- Räisänen J (2007) How reliable are climate models? *Tellus Series a-Dynamic Meteorology and Oceanography* 59(1):2–29
- Reichler T, Kim J (2008) How well do coupled models simulate today’s climate? *Bull Am Meteorol Soc* 89(3):303–311
- Robertson AW, Lall U, Zebiak SE, Goddard L (2004) Improved combination of multiple atmospheric GCM ensembles for seasonal prediction. *Mon Weather Rev* 132(12):2732–2744
- Robine J-M, Cheung SLK, Le Roy S, Van Oyen H, Griffiths C, Michel J-P, Herrmann FR (2008) Death toll exceeded 70,000 in Europe during the summer of 2003. *Comptes Rendus Biologies* 331(2):171–178
- Sheffield J, Wood EF, Roderick ML (2012) Little change in global drought over the past 60 years. *Nature* 491(7424):435–438
- Sun Q, Miao C, Duan Q, Kong D, Ye A, Di Z, Gong W (2014a) Would the ‘real’ observed dataset stand up? A critical examination of eight observed gridded climate datasets for China. *Environ Res Lett* 9(1): 015001
- Sun Q, Kong D, Miao C, Duan Q, Yang T, Ye A, Di Z, Gong W (2014b) Variations in global temperature and precipitation for the period of 1948 to 2010. *Environ Monit Assess* 186(9):5663–5679
- Sun Q, Miao C, Duan Q (2015) Projected changes in temperature and precipitation in ten river basins over China in 21st century. *Int J Climatol* 35:1125–1141. doi:10.1002/joc.4043
- Tabari H, Hosseinzadeh Talaei P (2013) Moisture index for Iran: spatial and temporal analyses. *Glob Planet Chang* 100:11–19

- Taylor KE (2001) Summarizing multiple aspects of model performance in a single diagram. *Journal of Geophysical Research: Atmospheres* (1984–2012) 106(D7):7183–7192
- Tebaldi C, Knutti R (2007) The use of the multi-model ensemble in probabilistic climate projections. *Philos Trans A Math Phys Eng Sci* 365(1857):2053–2075
- Torres RR, Marengo JA (2013) Uncertainty assessments of climate change projections over South America. *Theor Appl Climatol* 112(1–2):253–272
- Tubiello FN, Soussana J-F, Howden SM (2007) Crop and pasture response to climate change. *Proc Natl Acad Sci* 104(50):19686–19690
- Wake DB, Vredenburg VT (2008) Are we in the midst of the sixth mass extinction? A view from the world of amphibians. *Proc Natl Acad Sci* 105(Supplement 1):11466–11473
- Weigel A, Liniger M, Appenzeller C (2008) Can multi-model combination really enhance the prediction skill of probabilistic ensemble forecasts? *Q J R Meteorol Soc* 134(630):241–260
- Wu J, Miao C, Zhang X, Yang T, Duan Q (2017a) Detecting the quantitative hydrological response to changes in climate and human activities. *Sci Total Environ* 586:328–337
- Wu J, Miao C, Yang T, Duan Q, Zhang X (2017b) Modeling streamflow and sediment responses to climate change and human activities in the Yanhe River, China. *Hydrol Res*. doi:10.2166/nh.2017.168
- Yang T, Gao X, Sellars SL, Sorooshian S (2015) Improving the multi-objective evolutionary optimization algorithm for hydropower reservoir operations in the California Oroville–Thermalito complex. *Environ Model Softw* 69:262–279
- Yang T, Gao X, Sorooshian S, Li X (2016) Simulating California reservoir operation using the classification and regression-tree algorithm combined with a shuffled cross-validation scheme. *Water Resour Res* 52(3):1626–1651
- Yang T, Asanjan AA, Welles E, Gao X, Sorooshian S, Liu X (2017) Developing reservoir monthly inflow forecasts using artificial intelligence and climate phenomenon information. *Water Resour Res* 53. doi:10.1002/2017WR020482
- Yapo PO, Gupta HV, Sorooshian S (1998) Multi-objective global optimization for hydrologic models. *J Hydrol* 204(1):83–97
- Zanis P, Kapsomenakis I, Philandras C, Douvis K, Nikolakis D, Kanellopoulou E, Zerefos C, Repapis C (2009) Analysis of an ensemble of present day and future regional climate simulations for Greece. *Int J Climatol* 29(11):1614–1633